Supplementary Information (SI) for Journal of Materials Chemistry C.

2D Elastic fluorinated donor–accepter type π-conjugated molecular crystals and its optical crystal-polymer hybrid film

Keigo Yano, [a] Takumi Matsuo, *[a,b] and Shotaro Hayashi *[a,b]

School of Engineering Science, Kochi University of Technology, Kami, Kochi 782-8502, Japan.

FOREST Center, Research Institute, Kochi University of Technology, Kami, Kochi 782-8502, Japan.

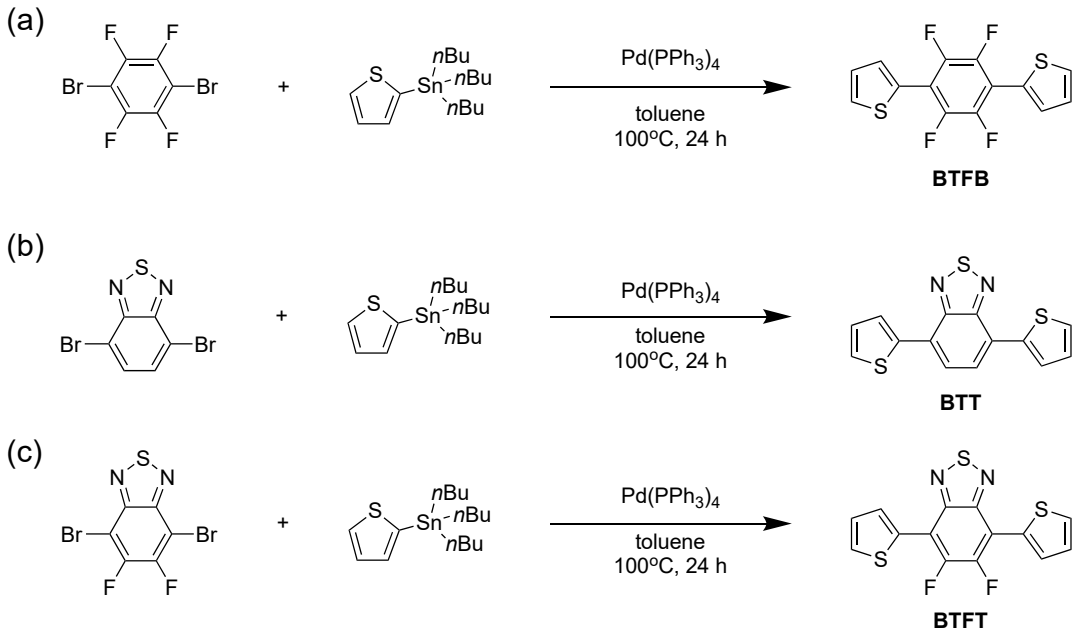

Figure S1. Synthetic scheme of (a) **BTFB**, (b) **BTT**, and (c) **BTFT**.

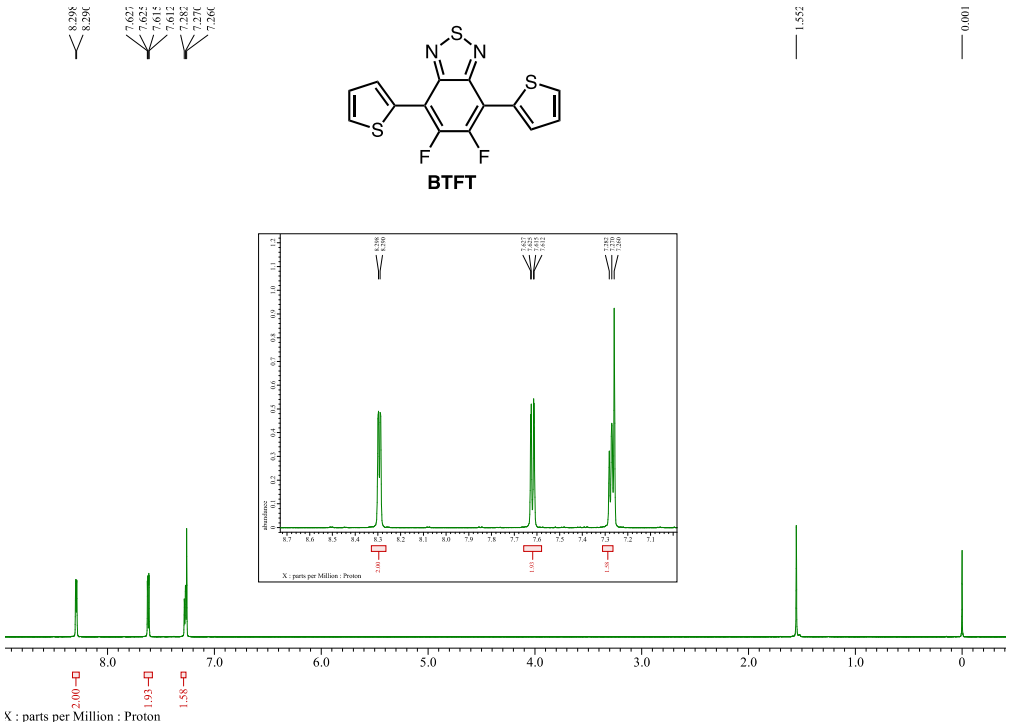

Figure S2. ^{1}H NMR spectrum of **BTFT** in $CDCl_3$.

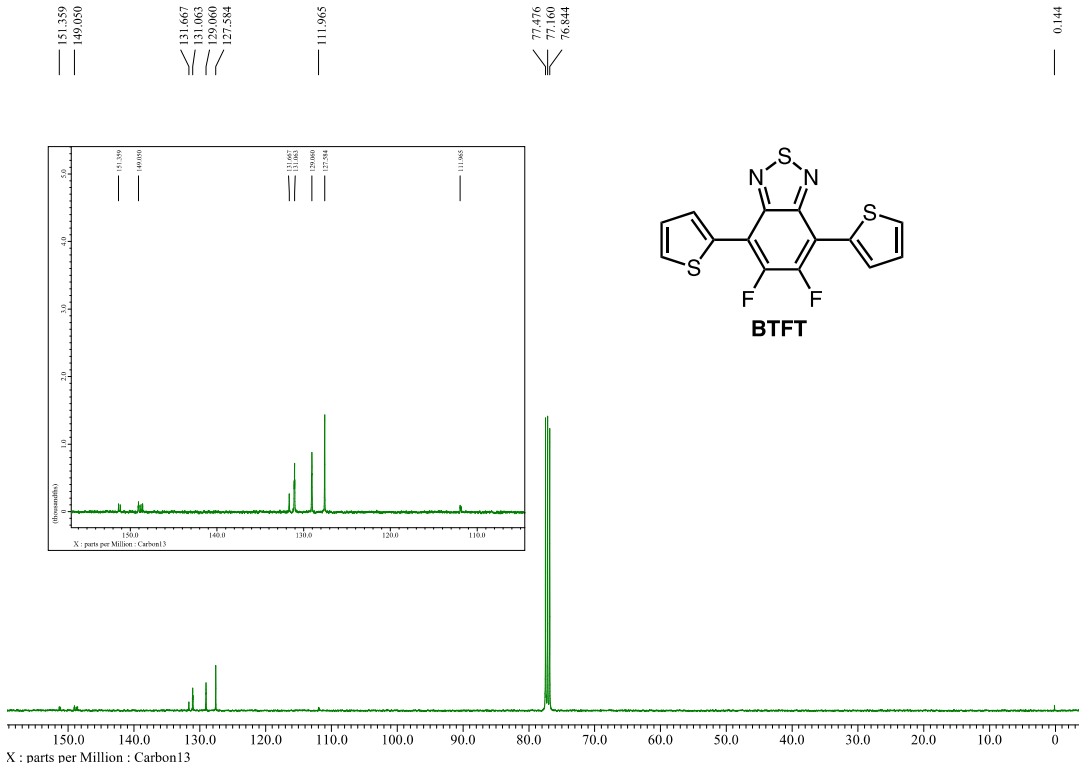

Figure S3. ^{13}C NMR spectrum of **BTFT** in $CDCl_3$.

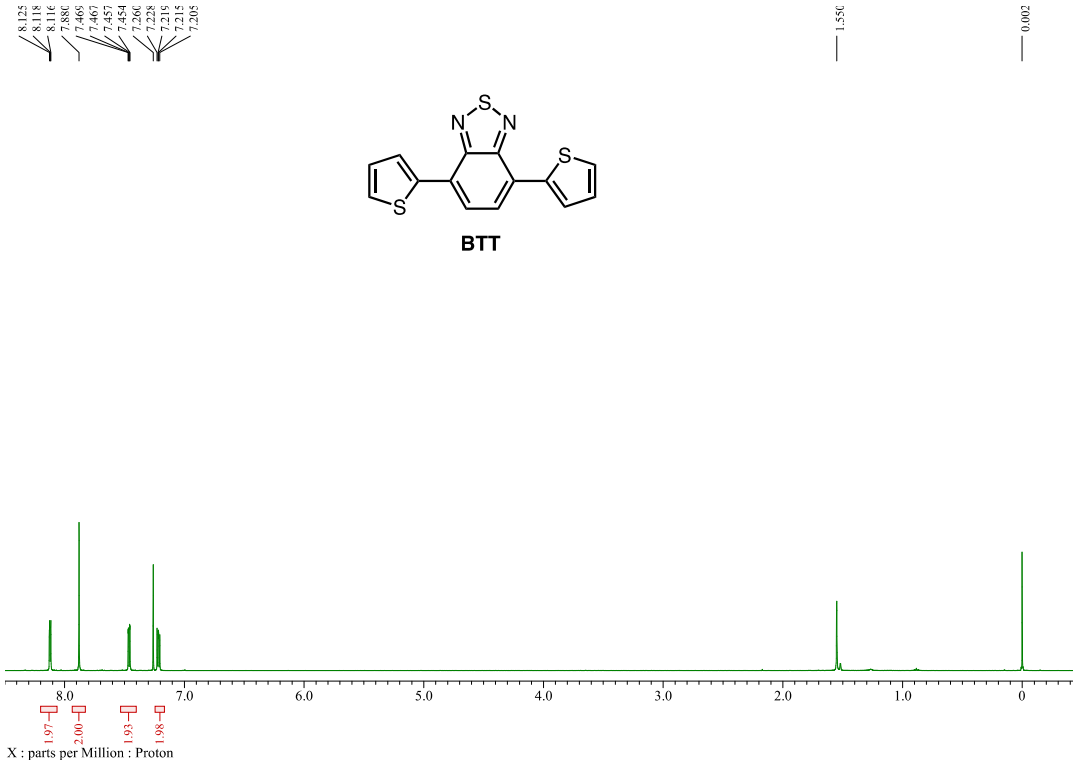

Figure S4. ^{1}H NMR spectrum of **BTT** in $CDCl_3$.

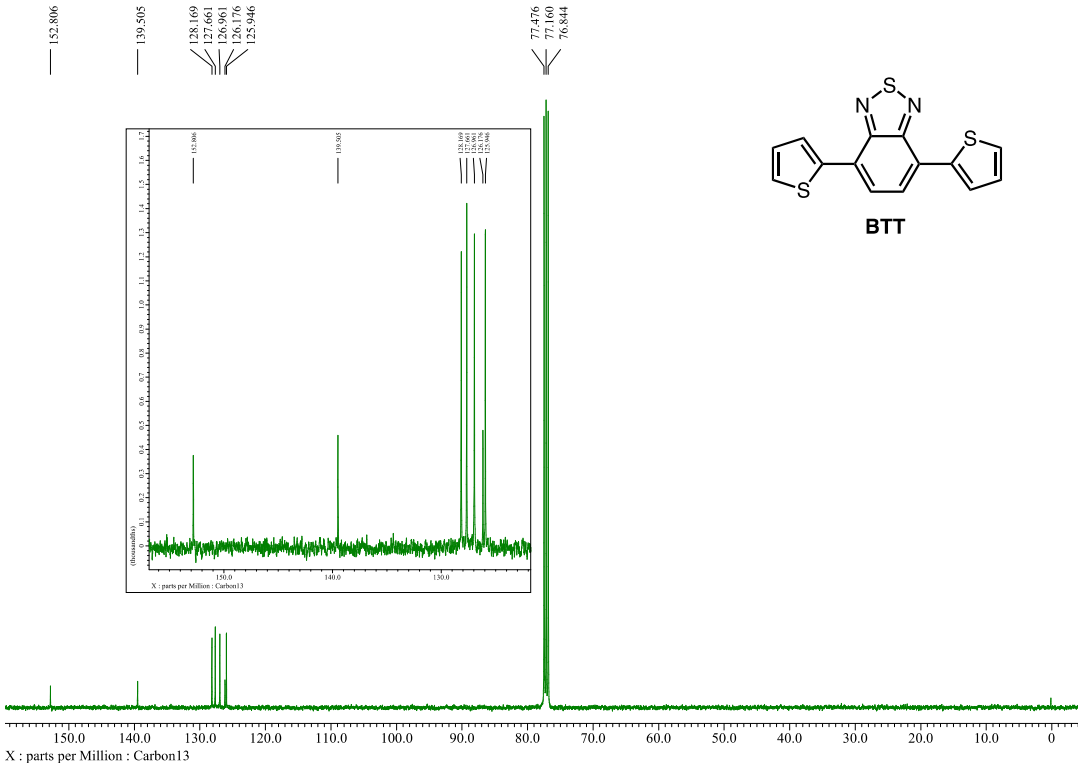

Figure S5. ^{13}C NMR spectrum of **BTT** in $CDCl_3$.

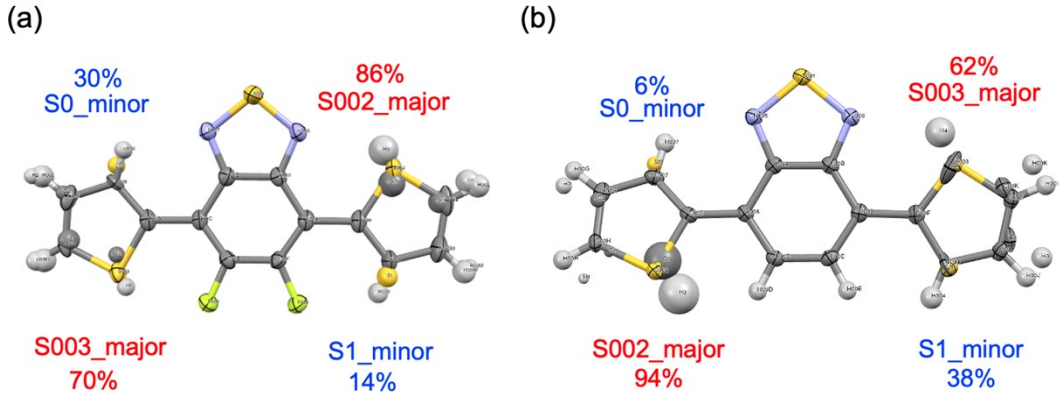

Figure S8. Molecular structure of (a) **BTFT** and (b) **BTT** (major and minor part of disorder assembly shown).

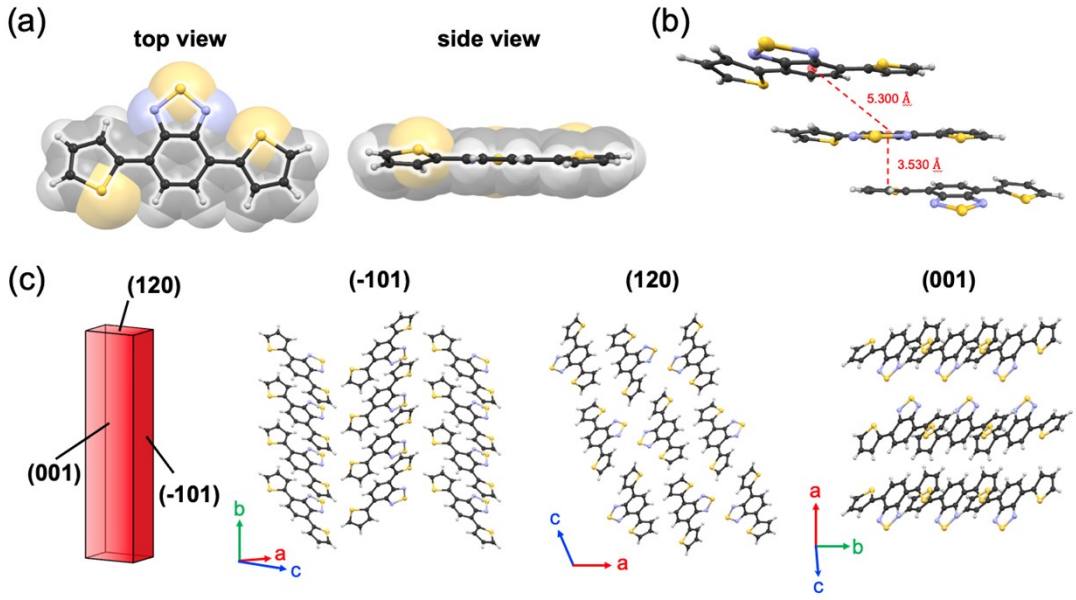

Figure S9. (**a**) Molecular structure (top and side views, respectively) of **BTT** in the crystal. (**b**) Slip-stacked structure, *J*-aggregate, of **BTT** in the crystal. (**c**) 3D crystal structure of the crystal **BTT**.

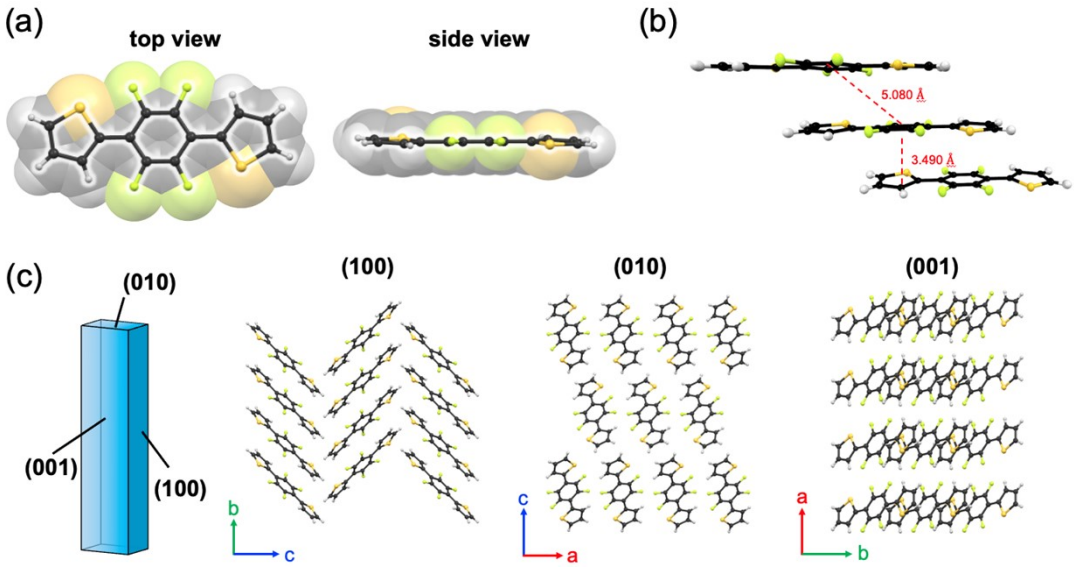

Figure S10. (**a**) Molecular structure (top and side views, respectively) of **BTFB** in the crystal. (**b**) Slip-stacked structure, *J*-aggregate, of **BTFB** in the crystal. (**c**) 3D crystal structure of the crystal **BTFB**.

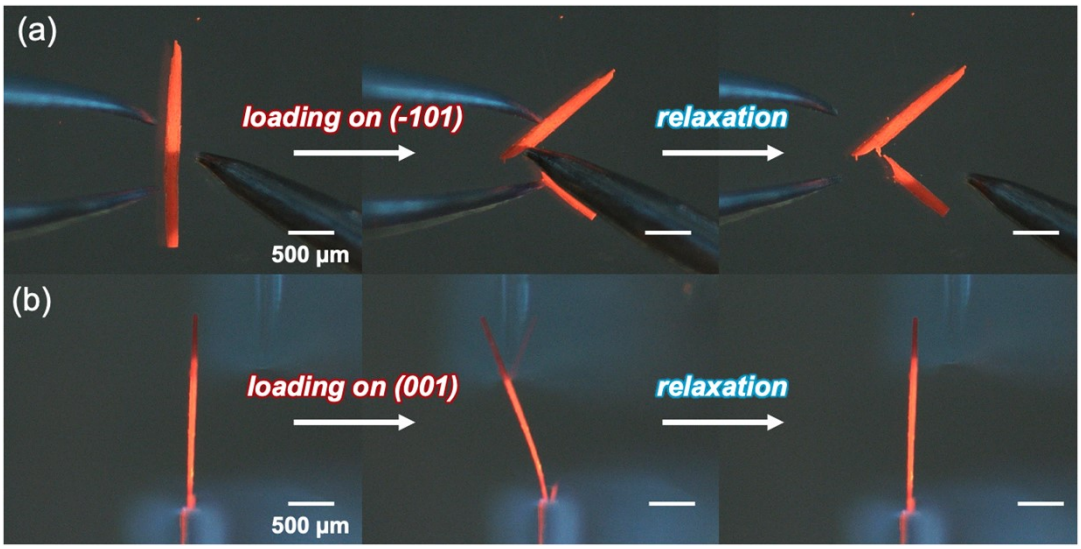

Figure S11. Mechanical deformation of **BTT** crystal. (a) Applied stress in the loading on (-101) face. (b) Applied stress in the loading on (001) face.

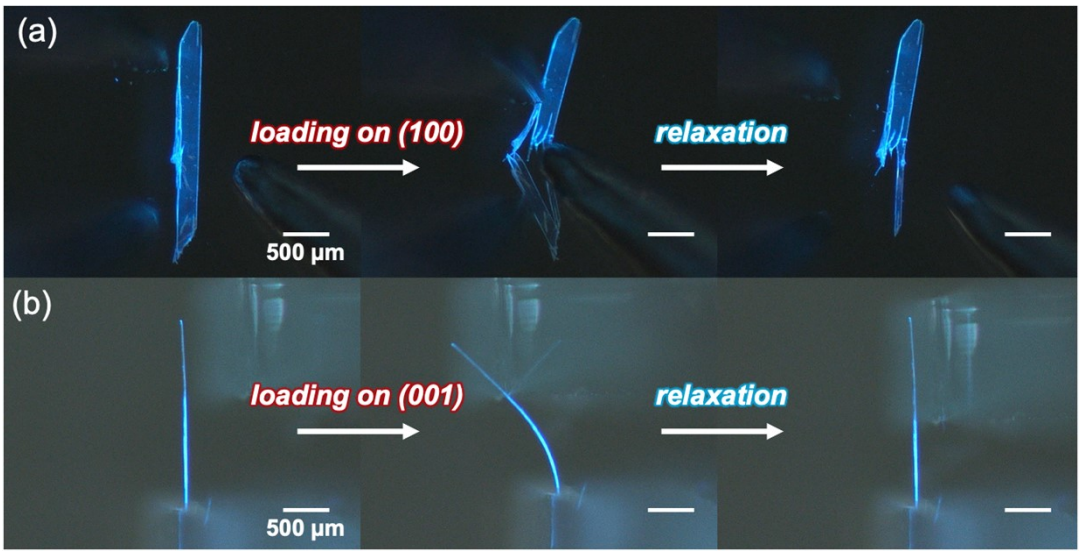

Figure S12. Mechanical deformation of **BTFB** crystal. (a) Applied stress in the loading on (100) face. (b) Applied stress in the loading on (001) face.

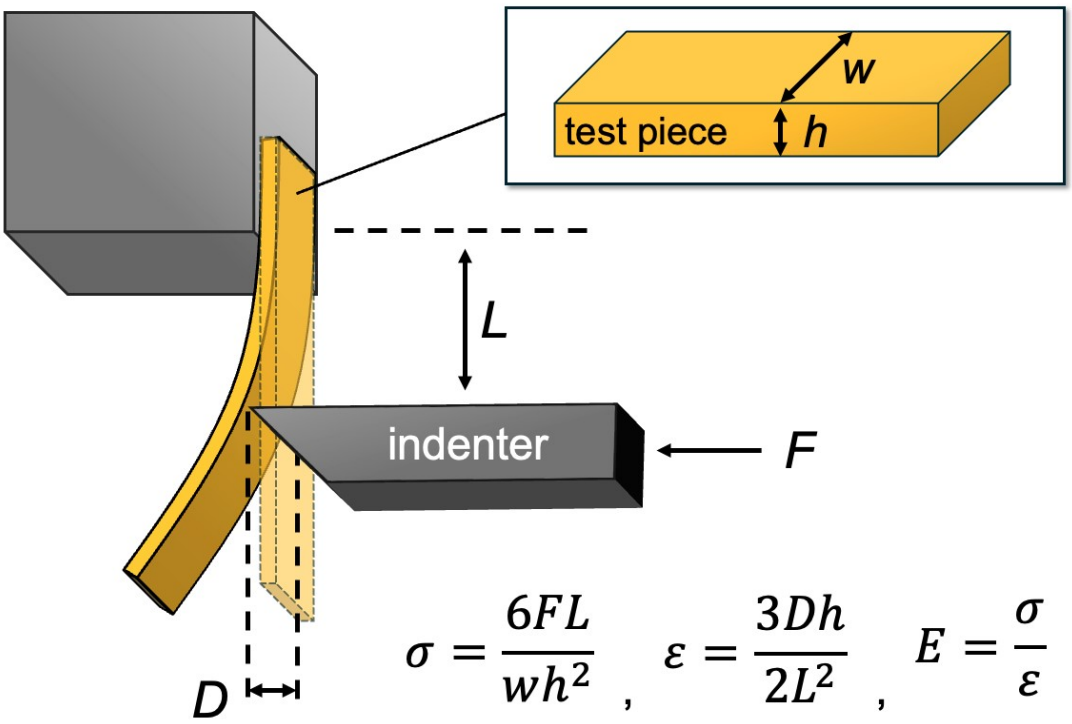

Figure S13. Schematic illustration of the cantilever test.

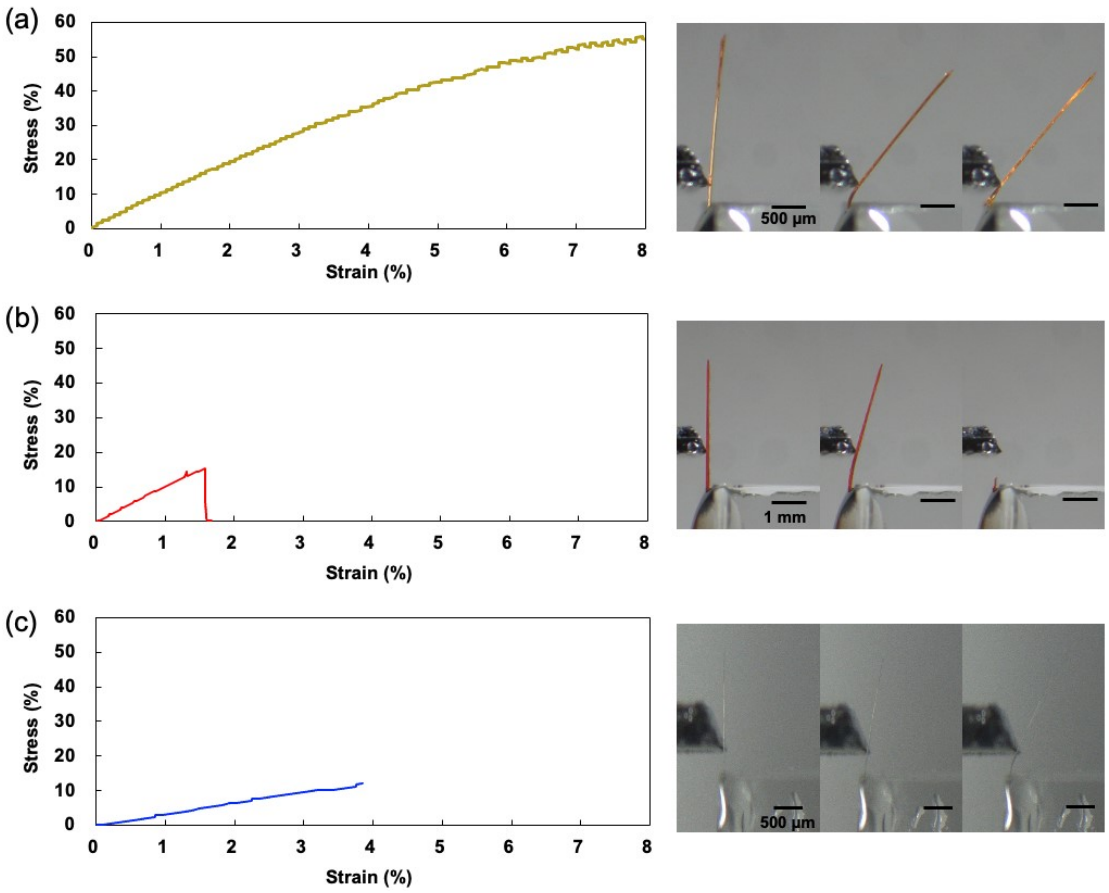

Figure S14. The F–S curves of (a) **BTFT**, (b) **BTT**, and (c) **BTFB** crystals along the *c*–axis.

Table S1. Indentation test on the *c*–axis of **BTFT**, **BTT**, **BTFB** crystals, measured young's modulus (***E***) and elastic limit (S_{lim})

	E **(GPa)**	S_{lim} **(%)**
BTFT	1.168 ± 0.362	4.29 ± 1.41
BTT	0.757 ± 0.683	1.54 ± 0.37
BTFB	0.306 ± 0.031	3.00 ± 0.21

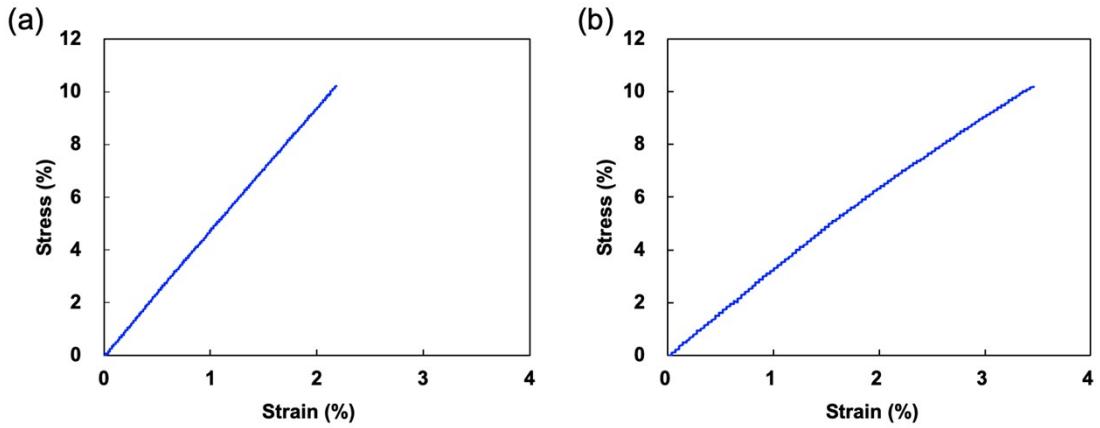

Figure S15. The F–S curves of (a) **PET** and (b) **PS** resin.

Table S2. Indentation test of **PET** and **PS** resin, measured young's modulus (***E***) and elastic limit (S_{lim})

	E **(GPa)**	S_{lim} **(%)**
PET	0.572± 0.106	–
PS	0.349 ± 0.036	–

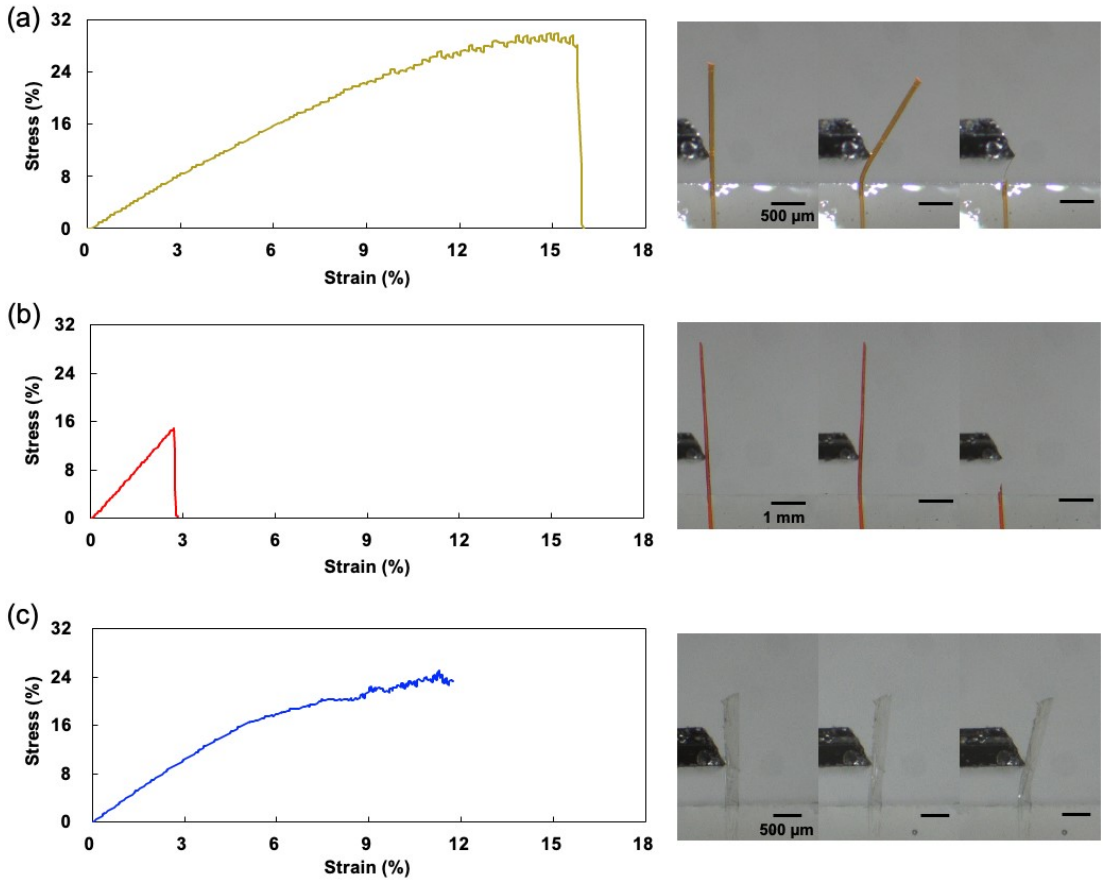

Figure S16. The F–S curves of (a) **BTFT**, (b) **BTT**, and (c) **BTFB** crystals along the *a*–axis.

Table S3. Indentation test on the *a*–axis of **BTFT**, **BTT**, **BTFB** crystals, measured young's modulus (***E***) and elastic limit (S_{lim})

	E **(GPa)**	S_{lim} **(%)**
BTFT	0.406 ± 0.119	7.50 ± 0.85
BTT	0.526 ± 0.048	2.40 ± 0.40
BTFB	0.374 ± 0.076	3.27 ± 0.19

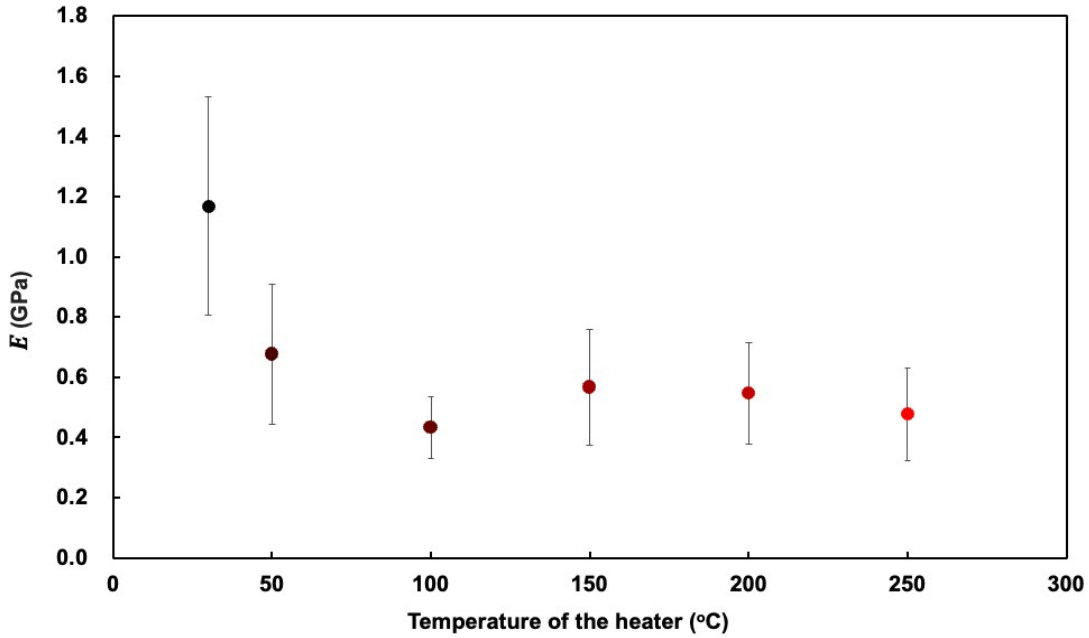

Figure S17. Temperature–dependance of Young's modulus for **BTFT** crystals from 30°C to 250°C.

Table S4. Temperature–dependance of Young's modulus for **BTFT** crystals

Temp. (°C)	*E* (GPa)
30	1.168 ± 0.362
50	0.676 ± 0.232
100	0.433 ± 0.103
150	0.557 ± 0.191
200	0.547 ± 0.168
250	0.476 ± 0.154

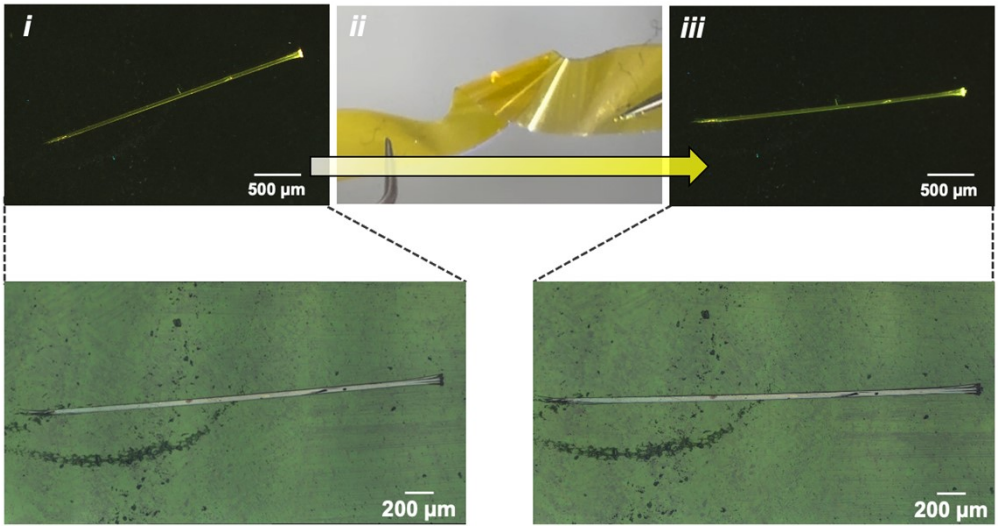

Figure S18. BTFT crystalline surfaces before and after applying mechanical stress to the hybrid material of crystalline **BTFT** and polyimide film. (i) Photograph of a crystal-polymer hybrid under UV irradiation. (ii) Mechanical deformation. (iii) State of a crystal under UV irradiation after mechanical stress.

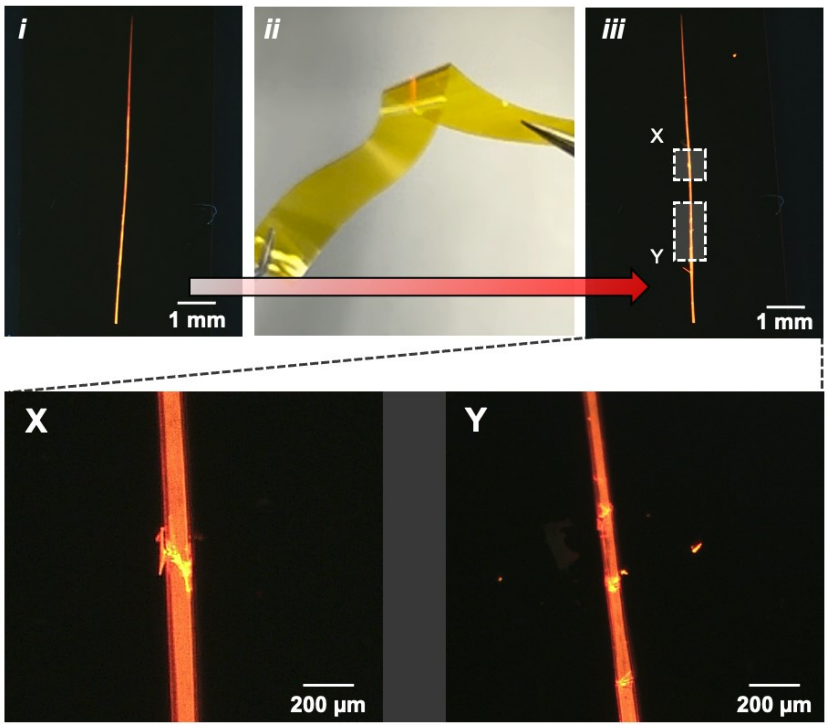

Figure S19. Crystalline **BTT** and polyimide film hybrid material and crystalline **BTT** surface after mechanical stress is applied. (i) Photograph of a crystal-polymer hybrid under UV irradiation. (ii)

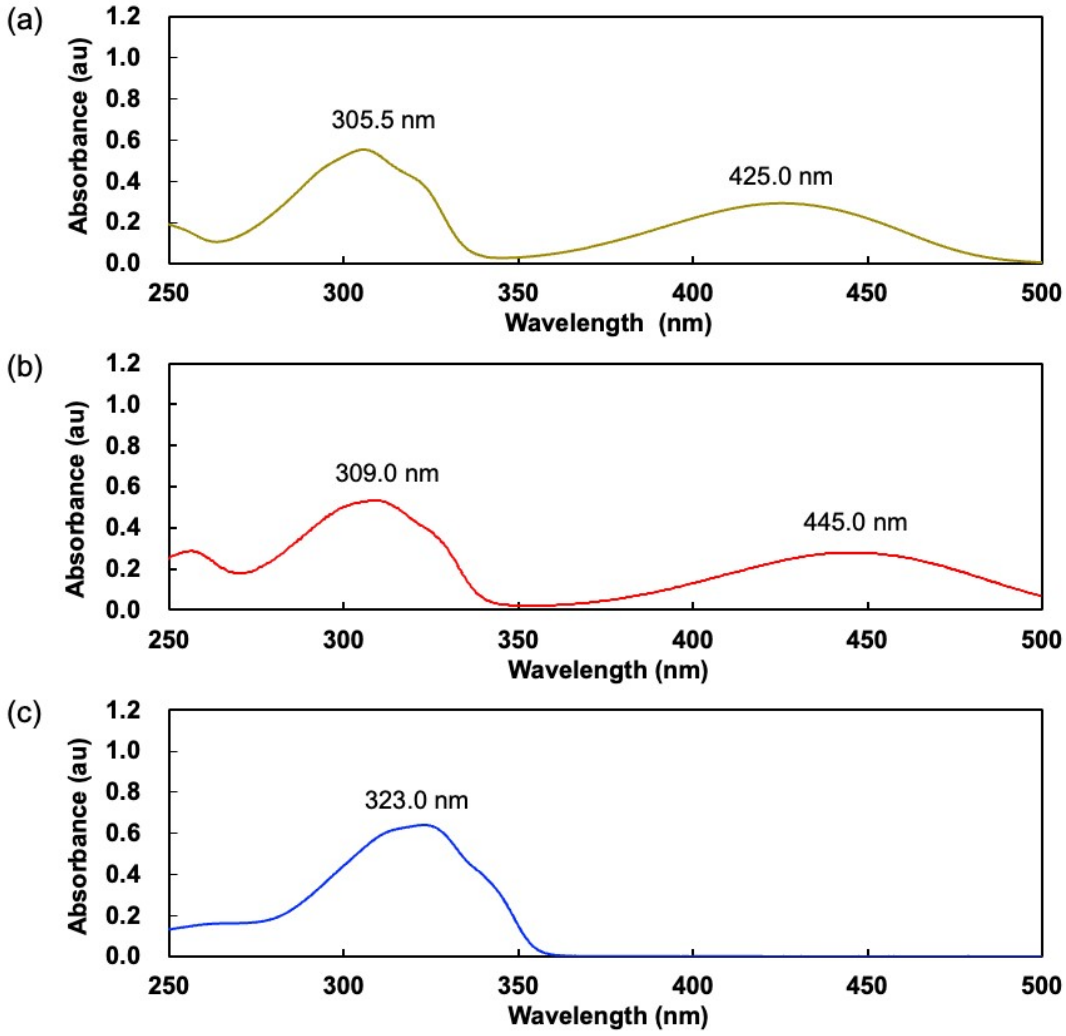

Figure S20. Absorption spectra of (a) **BTFT**, (b) **BTT** and (c) **BTFB** in CH_2Cl_2.

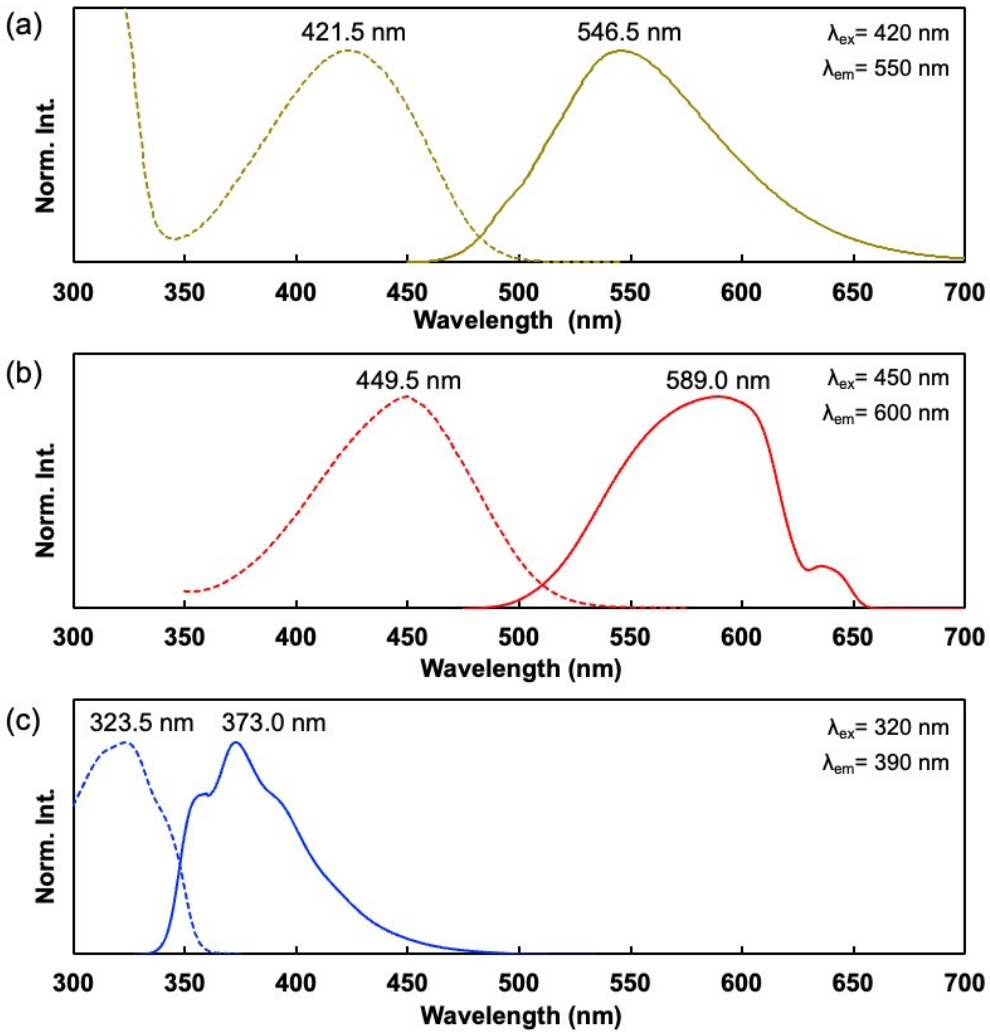

Figure S19. PL (–) and excitation (---) spectra of (a) **BTFT**, (b) **BTT** and (c) **BTFB** in CH_2Cl_2.

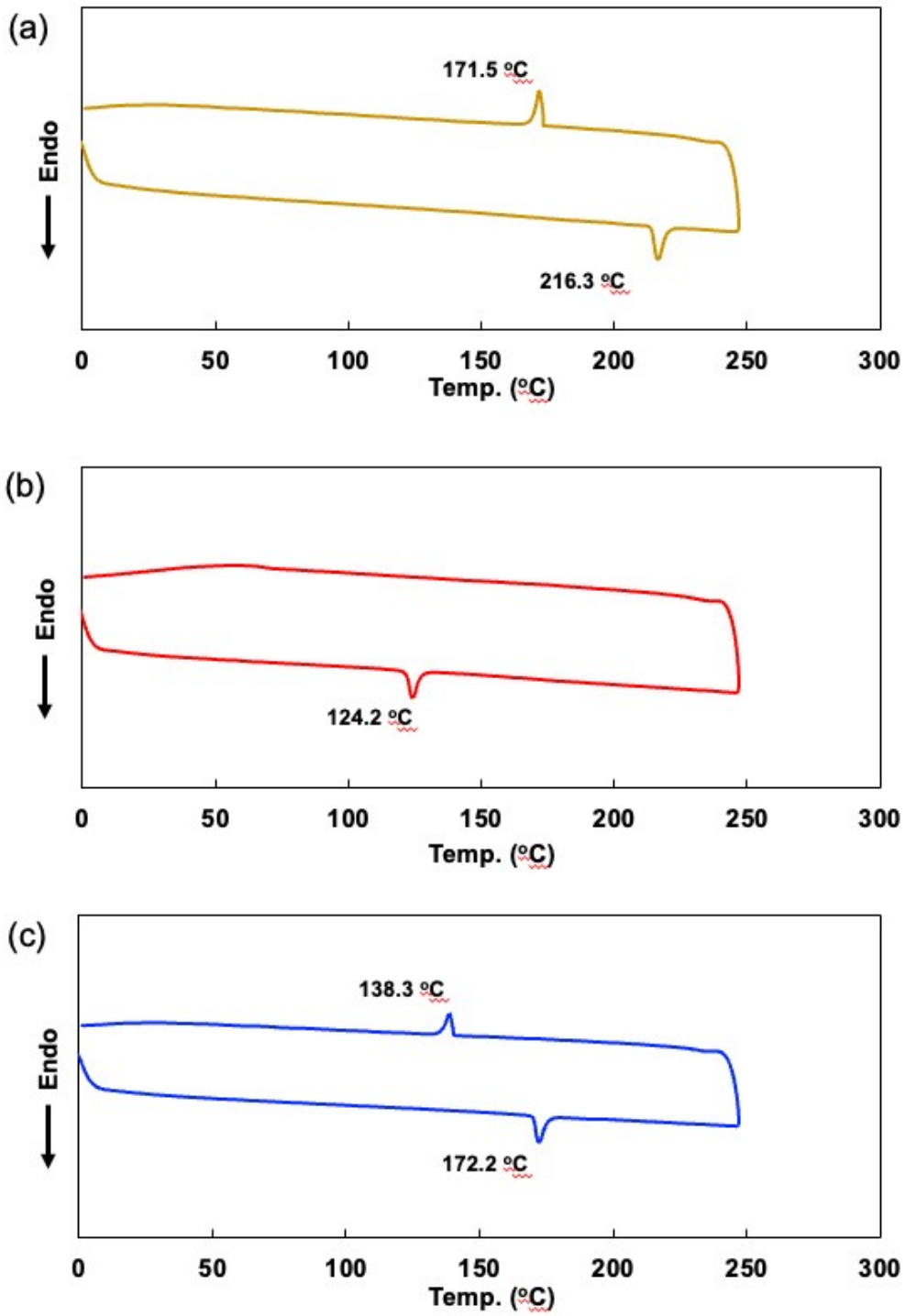

Figure S22. DSC analysis of (a) **BTFT**, (b) **BTT**, and (c) **BTFB** crystals.

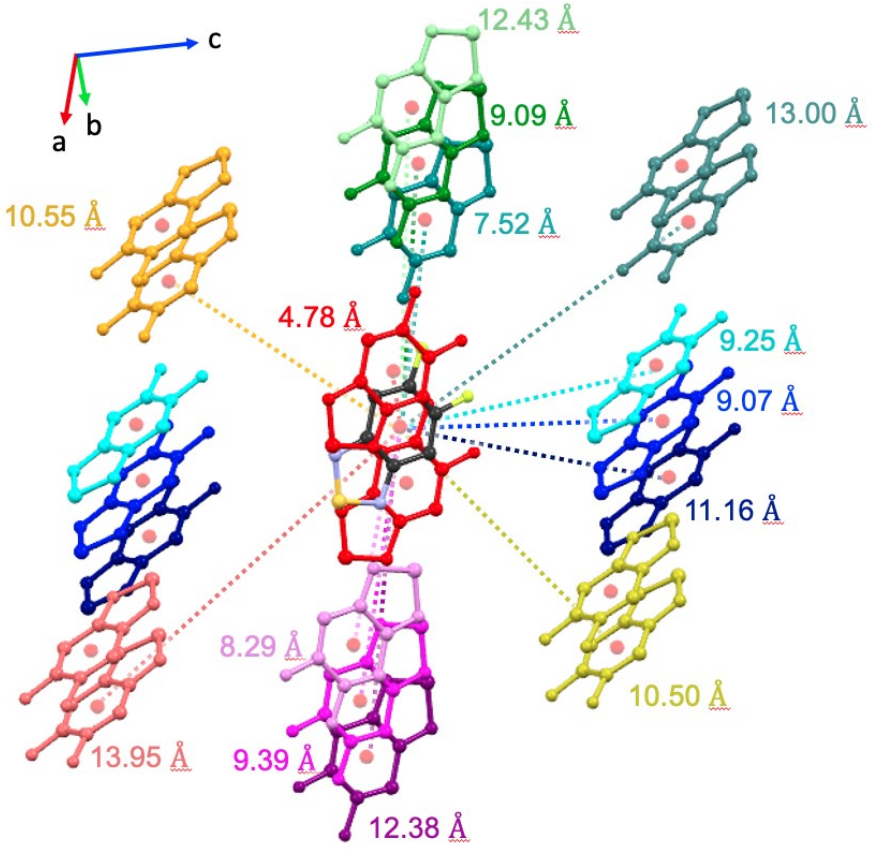

Figure S23. Crystal structure and center-to-center distance between nearby molecules of **BTFT** crystals.

Table S5. Transfer integral calculation results **BTFT** crystals

Center-to-center distance (Å)	Transfer integral	
	t_{hole} (meV)	$t_{electron}$ (meV)
4.78	52.25	53.20
7.52	1.22	1.50
8.29	0.81	61.63
9.07	13.06	14.15
9.09	2.31	1.50
9.25	57.69	52.52
9.39	1.22	21.09
10.50	61.09	47.08
10.55	78.23	61.36
11.16	15.65	34.01
12.38	0.27	0.68
12.43	0.54	0.68
13.00	1.36	0.41
13.95	1.36	2.72

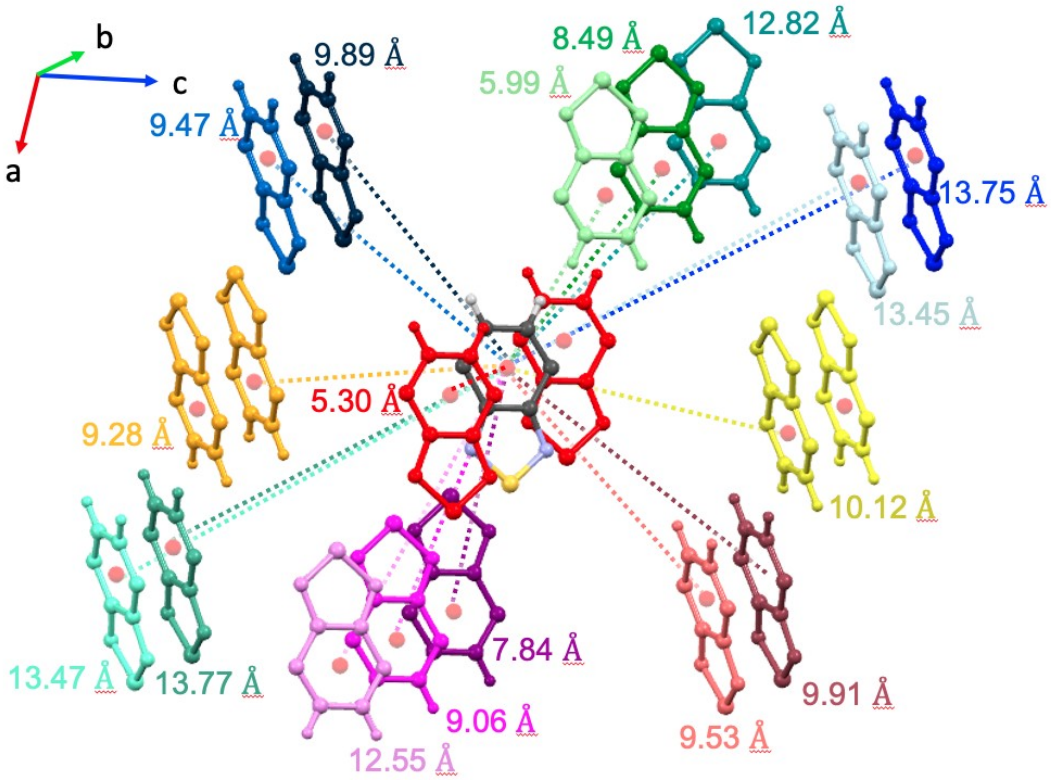

Figure S24. Crystal structure and center-to-center distance between nearby molecules of **BTT** crystals.

Table S6. Transfer integral calculation results **BTT** crystals

Center-to-center distance (Å)	Transfer integral	
	t_{hole} (meV)	$t_{electron}$ (meV)
5.30	47.89	40.41
5.99	19.32	48.57
7.84	3.95	47.08
8.49	3.27	5.85
9.06	1.22	41.77
9.28	89.53	75.78
9.47	63.27	62.45
9.53	63.27	62.99
9.89	8.98	5.71
9.91	8.44	4.63
10.12	95.24	66.67
12.55	3.81	47.08
12.82	3.81	47.08
13.45	13.33	5.58
13.47	7.76	6.80
13.75	19.32	18.10
13.77	19.32	17.42

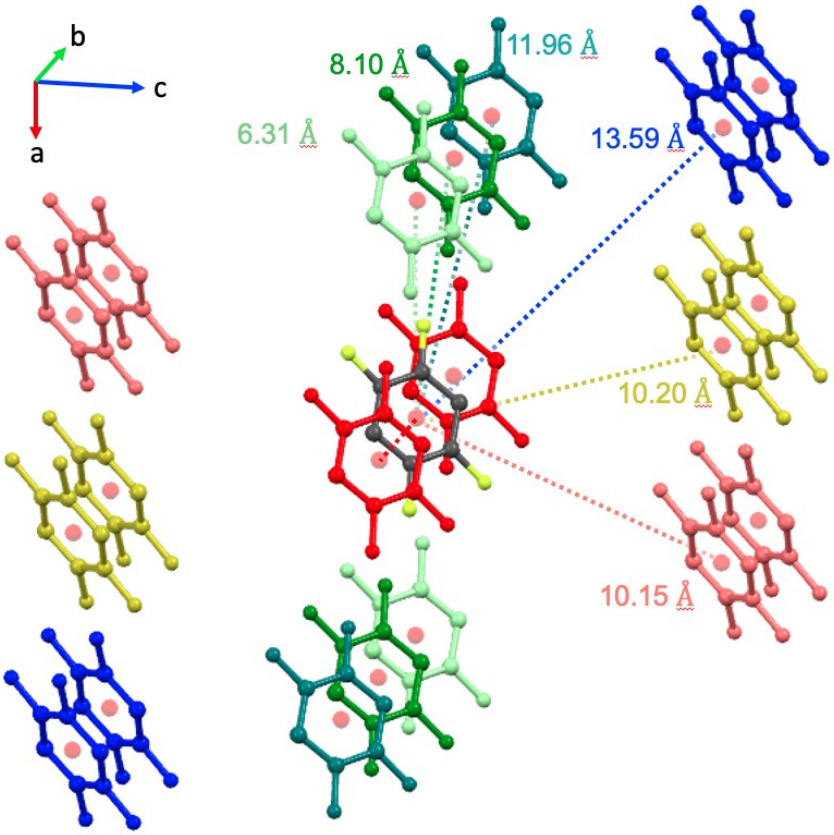

Figure S25. Crystal structure and center-to-center distance between nearby molecules of **BTFB** crystals.

Table S7. Transfer integral calculation results **BTFB** crystals

Center-to-center distance (Å)	Transfer integral	
	t_{hole} (meV)	$t_{electron}$ (meV)
5.08	37.82	89.66
6.31	5.03	1.63
8.10	0.54	0.54
10.15	52.10	52.65
10.20	87.08	82.99
11.96	0.14	0.14
13.59	8.98	7.35